

On Domain Decomposition for a Three-dimensional Extrusion Model

M. S. Eikemo

1 Introduction

The thermo-mechanical properties of aluminium during an extrusion process is described by a coupled set of nonlinear partial differential equations. The model is three-dimensional in order to support practical applications, and consists of a temperature equation, a continuity equation, and Navier-Stokes equations with a nonlinear Zener-Hollomon material law. The convective part is discretized in a Lagrangian sense using a modified method of characteristics. The equations are linearized in a straightforward manner, and we use a mixed finite element discretization with quadratic hexahedral elements for the approximation of velocities and linear hexahedral elements for temperature and pressure. After some decoupling, a positive definite system of linear equations for temperature and an indefinite block system for velocity and pressure are obtained. We use overlapping Schwarz domain decomposition methods in combination with a Krylov subspace accelerator to solve the problem. These techniques are powerful methods for solving problems on complex geometries, as they allow the possibility of local refinement at locations where the systems experience large gradients.

2 Model Description

For a domain $\Omega \subset R^3$ the fully scaled system of equations describing an extrusion process is given as

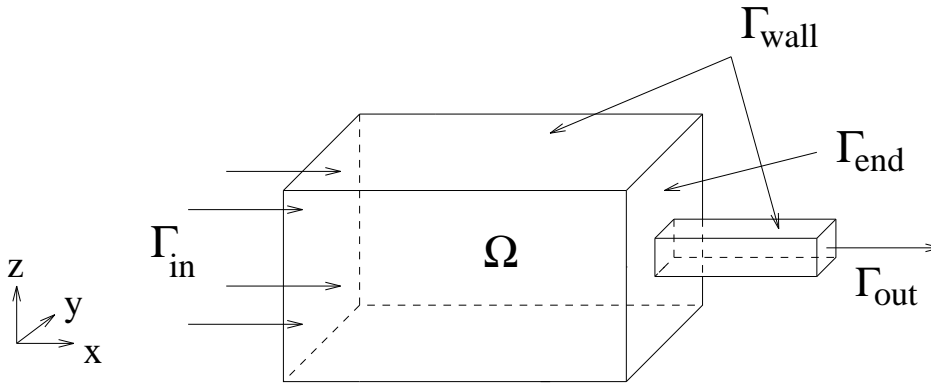
$$\begin{aligned} \text{Re} \left(\frac{\partial \mathbf{u}}{\partial t} + \mathbf{u} \cdot \nabla \mathbf{u} \right) &= -\nabla p + \nabla \cdot \boldsymbol{\tau} && \text{in } \Omega, \\ \nabla \cdot \mathbf{u} &= 0 && \text{in } \Omega, \\ \text{Pe} \left(\frac{\partial \theta}{\partial t} + \mathbf{u} \cdot \nabla \theta \right) &= \nabla^2 \theta + \beta \epsilon : \boldsymbol{\tau} && \text{in } \Omega, \end{aligned} \quad (2.1)$$

where dyadic notation is used for the last term, $\epsilon : \boldsymbol{\tau} = \epsilon_{ij} \tau_{ij}$. The primary variables are the velocity $\mathbf{u} = (u_1 \ u_2 \ u_3)^T$, the pressure p , and the temperature θ . Further, $\boldsymbol{\tau} = 2\mu\boldsymbol{\epsilon}$ is the stress tensor, where $\mu = \bar{\tau}/(3\bar{\epsilon})$ is the nonlinear viscosity coefficient. The effective strain rate is given by $\bar{\epsilon} = (\frac{2}{3}\boldsymbol{\epsilon} : \boldsymbol{\epsilon})^{\frac{1}{2}}$, where $\boldsymbol{\epsilon} = \frac{1}{2}(\nabla \mathbf{u} + \nabla \mathbf{u}^T)$ is the strain rate tensor. The viscosity coefficient also contains the Zener-Hollomon material model $\bar{\tau}(\bar{\epsilon}, \theta) = \alpha^{-1} \text{arcsinh}((Z/K)^{\frac{1}{m}})$, where α , A and m are material parameters and Z is the Zener-Hollomon parameter given by $Z = Z(\bar{\epsilon}, \theta) = \bar{\epsilon} \exp(Q/(R\theta))$, with Q denoting activation energy and R denoting the universal gas constant. The Reynolds number and the Péclet number are denoted by Re and Pe , respectively. For a more thorough presentation of the equations and the scaling procedure we refer to [Eik96], and topics concerning the extrusion process itself are discussed in [HSH92, HGS92] and references therein.

From specific material- and problem-dependent parameters we get the Reynolds number to be very small, typical of magnitude 10^{-8} . We may therefore neglect the left side of the vector equation in (2.1). Note that the equation still is nonlinear through the stress tensor.

Our computational domain is shown in Figure 1 and has a narrow channel to mimic the effect of an extrusion tool and a boundary $\partial\Omega = \Gamma_{\text{in}} \cup \Gamma_{\text{out}} \cup \Gamma_{\text{wall}} \cup \Gamma_{\text{end}}$. We use

Figure 1 Computational domain, with $\Gamma_{\text{wall}} = \partial\Omega \setminus (\Gamma_{\text{in}} \cup \Gamma_{\text{out}} \cup \Gamma_{\text{end}})$.



a no-slip condition for the velocity on Γ_{wall} and also zero velocity on Γ_{end} . Indicating the moving ram, the velocity is given a constant value in the x -direction on Γ_{in} . For the temperature the initial values are used on $\Gamma_{\text{in}} \cup \Gamma_{\text{wall}} \cup \Gamma_{\text{end}}$.

The pressure and velocity are slowly varying over a time step relative the variation of the temperature. We decouple the heat balance equation from the other equations by, on each time level, using a sequential iterative solution procedure. The boundary value problem for velocity-pressure can be stated as follows,

$$\begin{aligned} -\nabla \cdot \boldsymbol{\tau} + \nabla p &= 0 && \text{in } \Omega, \\ \nabla \cdot \mathbf{u} &= 0 && \text{in } \Omega, \\ \mathbf{u}(\mathbf{x}) &= \mathbf{f}(\mathbf{x}) && \text{on } \partial\Omega \setminus \Gamma_{\text{out}}, \\ p(\mathbf{x}) &= 0 && \text{on } \Gamma_{\text{out}}. \end{aligned} \quad (2.2)$$

and the initial boundary value problem for the temperature, with I being a time interval,

$$\begin{aligned} \text{Pe} \left(\frac{\partial \theta}{\partial t} + \mathbf{u} \cdot \nabla \theta \right) &= \nabla^2 \theta + \beta \boldsymbol{\epsilon} : \boldsymbol{\tau} && \text{in } I \times \Omega, \\ \mathbf{u}(\mathbf{x}) &= \mathbf{f}(\mathbf{x}) && \text{in } \Omega, \\ \theta(\mathbf{x}, t) &= g(\mathbf{x}) && \text{on } \partial\Omega \setminus \Gamma_{\text{out}} \quad \forall t, \\ \theta(\mathbf{x}, 0) &= \theta_0(\mathbf{x}) && \text{in } \Omega \text{ at } t = 0. \end{aligned} \quad (2.3)$$

3 Solution Procedure

The discretization for the velocity-pressure system (2.2) is carried out by a mixed finite element method, [Cia78, DJEW83, GR86, ELRV89, DES92], using hexahedral elements with triquadratic approximation for each of the velocity components and trilinear approximation for pressure, also called the hexahedral version of the $Q_2 - Q_1$ element. The linearization is handled by Picard iterations.

Carrying out the procedure described in [Eik96] results in a linear system $M\mathbf{y} = \mathbf{b}$, where the stiffness matrix has a block structure,

$$\begin{pmatrix} A_{11} & A_{12} & A_{13} & B_1^T \\ A_{21} & A_{22} & A_{23} & B_2^T \\ A_{31} & A_{32} & A_{33} & B_3^T \\ B_1 & B_2 & B_3 & 0 \end{pmatrix} \begin{Bmatrix} X \\ Y \end{Bmatrix} = \begin{pmatrix} A & B^T \\ B & 0 \end{pmatrix} \begin{Bmatrix} X \\ Y \end{Bmatrix} = \begin{Bmatrix} F \\ G \end{Bmatrix}. \quad (3.4)$$

The matrix $A = \{A_{ij}\}$, $i, j = 1, 2, 3$, is a 3-by-3 block matrix corresponding to the velocity components in the three momentum equations in (2.2). Since the matrix M is indefinite, the system (3.4) has to be reformulated in order for the preconditioned conjugate gradient method (PCG) to be applicable. In [BP94] a block preconditioning technique are introduced and we show in [Eik96] that this technique is efficient also for the extrusion problem. After some algebra on the rows, the system (3.4) is reformulated in such a way that the new coefficient matrix \tilde{M} is positive definite,

$$\tilde{M} \begin{Bmatrix} X \\ Y \end{Bmatrix} = \begin{Bmatrix} A_0^{-1} A & A_0^{-1} B^T \\ B A_0^{-1} (A - A_0) & B A_0^{-1} B^T \end{Bmatrix} \begin{Bmatrix} X \\ Y \end{Bmatrix} = \begin{Bmatrix} A_0^{-1} F \\ B A_0^{-1} F - G \end{Bmatrix}, \quad (3.5)$$

where A_0 is a preconditioner for A . The PCG method is now applicable, and as a preconditioner for this system,

$$\tilde{M}_0 = \begin{Bmatrix} I & 0 \\ 0 & \mathcal{K} \end{Bmatrix} \quad (3.6)$$

is used, where I is the identity matrix and \mathcal{K} is the preconditioner for the Schur complement $BA^{-1}B^T$,

$$\mathcal{K} = N_h + h^2I, \quad (3.7)$$

where h is the spatial resolution and N_h is the solution operator on the pressure grid for a finite element approximation to a Neumann problem, that is $w = N_h f$ satisfies $(\nabla w, \nabla \phi) = (f, \phi)$ for test functions ϕ . The theory in [BP94] shows that this preconditioner gives rise to convergence rates which can be bounded independently of the mesh size h . As a preconditioner for A we use a block-diagonal matrix A_0^{-1} with three copies of a preconditioner for the submatrix A_{11} on the diagonal, see [Eik96]. We have mostly been using incomplete factorization as preconditioner for A_{11} .

The discretization procedure for the temperature problem (2.3) is carried out in two steps. First, the hyperbolic part is solved by the modified method of characteristics (MMOC) and second, the resulting elliptic problem is discretized by the finite element method. Following the MMOC scheme in [Eik96] we get an elliptic equation with a known right-hand side, and the finite element approach results in a linear system

$$Ax = \mathbf{b}, \quad (3.8)$$

where the matrix A is positive definite and the PCG method is applicable. We have used both incomplete factorization and multigrid cycles as preconditioners.

4 Domain Decomposition

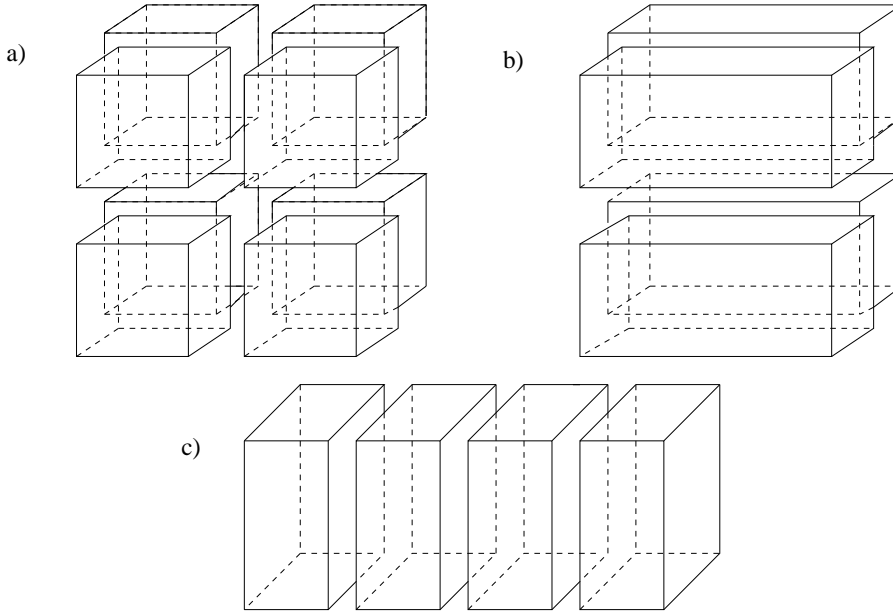
The extrusion problem is rich on localized phenomena, and domain decomposition methods prepare for local grid refinement. Near the extrusion tool at the outlet, with its complex structure with bridges and channels, large gradients in the flow pattern is produced. In order to capture these effects, the mesh is refined in these specific regions. In this way the size of the problem can be held at a minimum even with a high resolution in critical regions. Below we first show results from using additive and multiplicative Schwarz for different decompositions, and then present a local grid refinement technique. We refer to [BGS96] and references therein for a presentation of Schwarz methods and to [Sæv90, Sæv93, BEPS88, DEES90] for local grid refinement techniques.

Let the finite element space V^h be represented by the sum of N subspaces,

$$V^h = V_1^h + \dots + V_N^h, \quad (4.9)$$

where N is the number of subdomains, Ω_i . Following the presentation of the methods in [Eik96], the multiplicative and additive Schwarz methods take the forms of iterative

Figure 2 Different decompositions, a) (2,2,2), b) (1,2,2) and c) (4,1,1).



methods for solving

$$\left(I - \prod_{i=1}^N (I - P_i)\right)u_h = g_m \quad \text{and} \quad \left(\sum_{i=1}^N P_i\right)u_h = g_a, \quad (4.10)$$

respectively. Here $P_i : V^h \rightarrow V_i^h$ are orthogonal projections with respect to the bilinear form $a(\cdot, \cdot)$, and g_m and g_a are appropriate right-hand sides. The bilinear form $a(\cdot, \cdot)$ is appearing in the variational formulation of the problem to be solved, i.e. $a(u_h, \phi) = F(\phi)$ for test functions ϕ . For the heat equation it is defined like

$$a(\theta_h, \phi) = (\theta_h^{n+1, m+1}, \phi) + \frac{\Delta t}{\text{Pe}} (\nabla \theta_h^{n+1, m+1}, \nabla \phi) - \frac{\Delta t}{\text{Pe}} ((\beta \epsilon : \tau)_h^{n+1, m}, \phi) \quad (4.11)$$

where (\cdot, \cdot) denotes the usual L_2 -inner product and the superscript m counts the Picard iterations and n indicates the time step. Figure 2 shows examples of different ways to divide the domain Ω into subdomains Ω_i . The decomposition indicated by the pair (k, l, m) means to divide the domain into k parts along the x-direction, l parts along the y-direction and m parts along the z-direction, giving a total of $k \times l \times m$ subdomains. Consider the temperature problem (2.3). Table 1 gives results in terms of number of preconditioned conjugate gradient (PCG) iterations and condition number, κ , for both additive (AS) and symmetric multiplicative Schwarz (SMS) used as preconditioner. The time step is $\Delta t = 0.1$. The condition number is calculated from the Ritz values, see [Eik96], and the iterations are terminated when the discrete L_2 -norm of the residual is reduced by a factor $\epsilon_{CG} = 5 \cdot 10^{-8}$. The experiments support

Table 1 Number of PCG iterations with symmetric multiplicative Schwarz (SMS) and additive Schwarz (AS) preconditioners, and corresponding condition numbers, κ_m and κ_a . The three first columns give the number of elements in the x-, y- and z-directions, the kind of decomposition according to Figure 2 and the number of overlapping elements, respectively.

elements	decomposition	overlap	SMS	κ_m	AS	κ_a
32×32×32	(2,2,2)	1	5	1.41	14	22.41
		2	3	1.08	12	13.18
		3	3	1.02	10	10.58
	(1,2,2)	1	5	1.41	15	22.56
		2	3	1.07	12	13.24
		3	3	1.02	10	10.59
	(1,1,2)	1	5	1.34	10	6.24
		2	3	1.06	7	4.11
		3	2	1.01	6	3.49
	(2,1,1)	1	4	1.32	6	2.93
		2	2	1.05	4	2.58
		3	2	1.01	4	2.26
	(4,1,1)	1	4	1.37	7	3.11
		2	3	1.07	5	2.71
		3	2	1.02	5	2.31

the well known properties of the methods, see [Eik96]. Note also that the table show that the (1,2,2) decomposition has more in common with the (2,2,2) than with the (4,1,1), which is the other four-subdomain decomposition. This is reasonable since all the subdomains overlap each other in both cases. We also observe from the table that the results get worse when the decomposition has a division in the z-direction, especially for the additive preconditioner. By calculating the temperature field on Γ_{out} we invoke a Neumann condition on this boundary, and this condition, compared to a Dirichlet condition, makes greater demands on the system. Decompositions in the y- and z-directions result in several subdomains with a Neumann boundary, while decomposition in the x-direction only causes only one subdomain to have a Neumann boundary. This will be a topic for further investigation.

Consider now $\Omega \subset R^3$ to be the domain in Figure 3, consisting of a body and a narrow channel. We begin by introducing a coarse grid for Ω , with mesh size h_c . Then a fine grid according to a refinement level k is introduced, for which the mesh size is $h_f = 2^{-k}h_c$. The domain is divided into two subdomains, one covered with the coarse mesh and one with the fine mesh, see Figure 3. The triangulation leads to the introduction of a set of so-called slave nodes on the boundary surface of the refined region. The values of functions in the composite finite element space in these nodes are, because of the continuity assumption, completely determined by their values in neighbouring coarse-grid nodes. This also means that a discrete function is uniquely represented by a vector with entries corresponding to the genuine degrees of freedom,

Figure 3 Composite mesh for the domain $\Omega = \Omega_1 \cup \Omega_2$,
 $\partial\Omega = \Gamma_{\text{in}} \cup \Gamma_{\text{out}} \cup \Gamma_{\text{wall}} \cup \Gamma_{\text{end}}$.

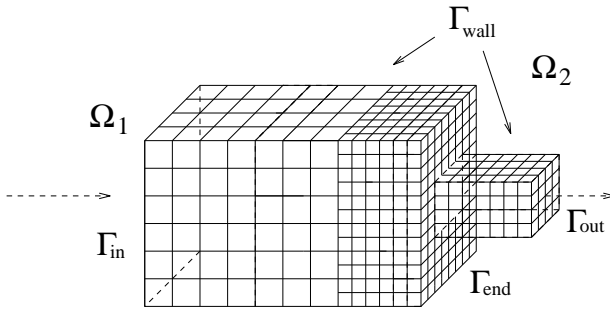
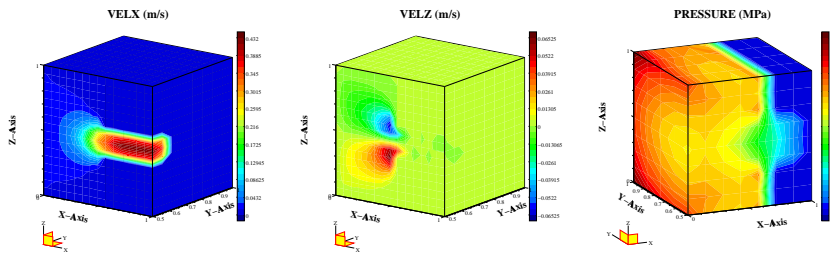


Figure 4 Domain consisting of $4 \times 8 \times 8$ elements and a narrow channel of $3 \times 2 \times 2$ elements. No-slip boundary condition $\mathbf{u}=0$ on Γ_{wall} , $u_1 = 1$ (0.015 m/s) on Γ_{in} , $u_3 = 0$ on Γ_{in} and $p = 0$ on Γ_{out} . The three subfigures show the x-component of the velocity, the z-component of the velocity and the pressure, respectively. Note that the last domain is turned compared to the other two.



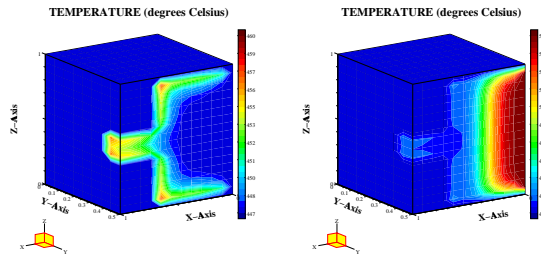
i.e. all nodes except the slave nodes. Let cross nodes denote the nodes on the interface which appear both in the coarse and the refined grid. By employing this refinement strategy the size of the problem is dramatically reduced compared to having a global fine grid.

We use the PCG method with SMS as a preconditioner. The subdomain structure can be utilized both in the matrix multiplication operation in the PCG algorithm and the preconditioning procedure. To avoid having to deal with the irregular global stiffness matrix, A , arising from the composite grid considered, the matrix is never explicitly completed. Instead it is considered as a set of submatrices, each submatrix referring to a certain subdomain Ω_i , see also [Sævn90]. Matrix multiplication will consist of operations on each of the subdomains separately, and then gluing the global product together along the interface. The SMS preconditioner utilizes in our case the same subdomains as was used to define the composite mesh, extending the refined region to define the overlap. In cases with more than one refined subdomain, however, the preconditioner may use subdomains consisting of some collection of refined regions. These procedures are given a more thorough presentation in [Eik96].

Results obtained with local refinement in the outlet region compared to global fine resolution are reported in [Eik96]. The dramatic changes in velocity occur in the outlet region and are properly resolved by the fine grid. For the temperature, where local behaviour is seen near Γ_{wall} in the whole domain, these effects are not properly resolved on a coarse grid. Similar for the pressure, rapid changes in values occur near the in-boundary. It is obvious that making the refinement technique adaptive will cause the effects to be properly resolved wherever they occur.

Figure 4 visualizes the solutions from solving (2.2) with $\mathbf{u} = (1 \ 0 \ 0)^T$ on Γ_{in} and $p = 0$ on Γ_{out} . The temperature is held constant at zero, i.e. 447 °C. Note that only half the domain is plotted in order to be able to see the behaviour of the solutions inside, along the flow direction. We see that u_1 has attained a domal profile with the largest values in the middle and decreasing to zero towards the surfaces making Γ_{wall} . This profile is also supported by the plot for u_3 , where there are negative values in the upper half of the domain and positive values in the lower half, showing flow downwards from the top and up from the bottom. We observe the largest pressure towards the boundaries around the inlet area, and especially in the corners, due to the boundary conditions $u_1 = 1$ on Γ_{in} and $u_1 = 0$ on Γ_{wall} . Figure 5 shows temperature results from solving (2.3) with a given velocity field $u_1 = \sin(\pi y)\sin(\pi z)$ for two cases of boundary values, see the figure text. We observe the two main effects, transportation and very local changes in gradients.

Figure 5 Temperature solutions after two time steps, $\Delta t = 0.1$. Domain with body consisting of $8 \times 16 \times 16$ elements and channel of $3 \times 4 \times 4$ elements. Boundary condition $\theta = 0$ (447 °C) on Γ_{in} and $\theta = 0$ (547 °C) on Γ_{in} , respectively.



5 Conclusions and Future Work

In this paper we have reported results obtained from applying domain decomposition methods to the extrusion problem. Together with local mesh refinement these methods proved to be very efficient techniques for reducing the size of the problem and at the same time obtaining the required accuracy.

Future activity involves both improvements of the solution methods and extensions of the model. The most obvious and most necessary improvement of the solution strategy is to make the grid refinement adaptive. Our numerical experiments show

the need for following temperature fronts in addition to handling more stationary local effects. Extensions of the model may be to involve more complex geometries and include input from the surroundings in terms of boundary conditions. A realistic die has a very complex geometry with hollow spaces and bridges and heat transfer between the metal and the container, ram and die do occur.

The programming language C++ offers several tools for supporting data abstraction and object-orientation. A further utilization of all the possibilities and subtleties of C++ would increase the efficiency of the implementation and make it applicable to more general models.

Acknowledgement

The support provided by Norsk Hydro is gratefully acknowledged.

REFERENCES

- [BEP88] Bramble J., Ewing R., Pasciak J., and Schatz A. (1988) *A preconditioning technique for the efficient solution of problems with local grid refinement*. *Comp. Meth. Appl. Mech. Eng.* 67: pp. 149–159.
- [BGS96] Bjørstad P., Gropp W., and Smith B. (1996) *Domain Decomposition: Parallel Multilevel Methods for Elliptic Partial Differential Equations*. Cambridge University Press.
- [BP94] Bramble J. and Pasciak J. (1994) *Iterative techniques for time dependent Stokes problems*. *Math. Comp.* .
- [Cia78] Ciarlet P. (1978) *The finite element method for elliptic problems*. North Holland Publishing Company.
- [DEES90] Dahle H., Espedal M., Ewing R., and Sævareid O. (1990) *Characteristic Adaptive Subdomain Methods for Reservoir Flow Problems*. *Numer. Meth. for Partial Differential Equations* 6: pp. 279–309.
- [DES92] Dahle H., Espedal M., and Sævareid O. (1992) *Characteristic local grid refinement for reservoir flow problems*. *Int. J. Numer. Meth. Eng.* 34: pp. 1051–1069.
- [DJEW83] Douglas J., JR, Ewing R., and Wheeler M. (1983) *The approximation of the pressure by a mixed method in the simulation of miscible displacement*. *RAIRO Anal. Numer.* 17: pp. 17–33.
- [Eik96] Eikemo M. (1996) *On Numerical Techniques and Characteristic Local Refinement for Simulating Aluminium Extrusion*. PhD thesis, Department of Mathematics, University of Bergen.
- [ELRV89] Ewing R., Lazarov R., Russel T., and Vassilevski P. (1989) *Local Refinement via Domain Decomposition Techniques for Mixed Finite Element Methods with Rectangular Raviart-Thomas Elements*. In 3rd International Symposium on Domain Decomposition Methods for Partial Differential Equations. SIAM.
- [GR86] Girault V. and Raviart P. (1986) *Finite Element Methods for Navier-Stokes Equations*. Springer-Verlag, Berlin Heidelberg.
- [HGS92] Herberg J., Gundesø K., and Skauvik I. (1992) *Application of Numerical Simulations in Design of Extrusion Dies*. In 5th International Alu. Extr. Techn. Seminar. Chicago, Illinois, USA.
- [HSH92] Holthe K., Støren S., and Hansen L. (1992) *Numerical simulation of the aluminium extrusion process in a series of press cycles*. In 4th International Conference on Numerical Methods in Industrial Forming Processes. Balkema.

- [Sæv90] Sævareid O. (1990) *On Local Grid Refinement Techniques for Reservoir Flow Problems*. PhD thesis, Department of Mathematics, University of Bergen.
- [Sæv93] Sævareid O. (1993) *Simulation of Extrusion combining Local Grid Refinement and Lagrangian time-marching*. In 8th International Conference on Finite Elements in Fluids. Pineridge Press, Barcelona.